Degradation study of malachite green on chitosan films containing heterojunctions of melon/TiO₂ absorbing visible-light in solid-gas interfaces

Juliana Pérez-Obando[a], Diego A. Marín-Silva[b], Adriana N. Pinotti[b,d], Luis R. Pizzio[c,*], Paula Osorio-Vargas[a], Julián A. Rengifo-Herrera[c,*]

[a] Universidad Tecnológica de Pereira, Escuela de Química, Pereira, Risaralda, 660003, Colombia
[b] Centro de Investigación y Desarrollo en Criotecnología de Alimentos (CIDCA), CONICET, La Plata, Facultad de Ciencias Exactas, UNLP, 47 y 116, 1900, La Plata, Argentina
[c] Centro de Investigación y Desarrollo en Ciencias Aplicadas "Dr. J.J. Ronco" (CINDECA), Departamento de Química, Facultad de Ciencias Exactas, UNLP-CCT La Plata, CONICET, 47 No. 257, 1900, La Plata, Buenos Aires, Argentina
[d] Facultad de Ingeniería, Universidad Nacional de La Plata, La Plata, Argentina

ABSTRACT

Urea modified TiO₂ nanoparticles were synthesized at different TiO₂: urea ratios (10, 30 and 60 (%wt) named UTiO₂-10, 30 and 60) by sol-gel method and annealing at 400 °C during 1 h. Characterization revealed the presence of TiO₂ nanoparticles with visible light absorption (between 400 and 500 nm) probably due by the formation of thermolysis urea byproducts such as melon, which may induce a TiO₂/melon heterojunction. Then, modified nanoparticles were immobilized on chitosan films by adding 30% (70QS/30UTiO₂) and 50% 50QS/50UTiO₂) of UTiO₂ nanoparticles. Functionalized films were characterized by SEM-EDS, DRS and AFM. Photo-induced degradation of malachite green stains was evaluated on these films under different wavelengths. Upon UV-A + visible light irradiation, films showed good activity even slightly better than those containing Evonik P-25 (70QS/30P-25). Upon visible light between 450 and 800 nm, films evidenced a satisfactory performance but slower than under UV-A + visible light irradiation whereas the photobleaching activity of 70QS/30P-25 was very poor. When visible light irradiation with wavelengths higher than 590 nm was used, a slight photobleaching was also observed. DRS spectra taken at different irradiation times showed that dye underwent N-demethylated oxidative reactions either upon UV–vis or visible light irradiation. ATR-FTIR measurements revealed the generation of benzophenones after 6 h of irradiation probably suggesting the formation of singlet oxygen under visible light. 70QS/30UTiO₂-10 films showed a good photo-bleaching activity after 18 h of continuous UV-A + visible light irradiation.

1. Introduction

Late in the 90 s, Wang et al. [1] reported for the first time the UV-light photoinduced superhydrophilicity of TiO₂ polycrystalline films and their applications as photoinduced self-cleaning surfaces. Self-cleaning properties are due to a synergic effect caused by both UV-light induced photocatalytic reactive oxygen species (ROS) generation over TiO₂ surfaces, which attack organic molecules adsorbed onto TiO₂ films, and superhydrophilicity leading to water droplet spreading [2,3]. On the other hand, TiO₂ either anatase or rutile is a semiconductor with a band gap energy around 3.0–3.2 eV, allowing the photo-induced ROS production only by UV irradiation, limiting its use as a self-cleaning material in solar and indoor applications. Studies reported in the literature have described several approaches to shift the TiO₂ light

absorption toward the visible region [4–8], one of them, the nitrogen doping have been extensively studied [9–15]. Since in 1986 Sato [16] reported for the first time the preparation of visible-light absorbing TiO₂ nanoparticles doped with NOₓ with high photocatalytic activity, an enormous amount of publications have appeared in the literature about this issue [9,10,19,20,11–18]. In 2001, Asahi et al. [21] coined for the first time the term "nitrogen doping" (N-doped) to call visible light active TiO₂₋ₓNₓ prepared by sputtering in N₂/Ar atmospheres. This study suggested by theoretical calculations using density of states (DOS) that the origin of its visible light absorption was a substitutional N-doping (O atoms replaced by N atoms) narrowing the band gap energy caused by mixing of O 2p with N 2p orbitals. Later, different studies published by Di Valentin et al. and Livraghi et al. [22–24] claimed that this visible light absorption of TiO₂ could be due to interstitial or
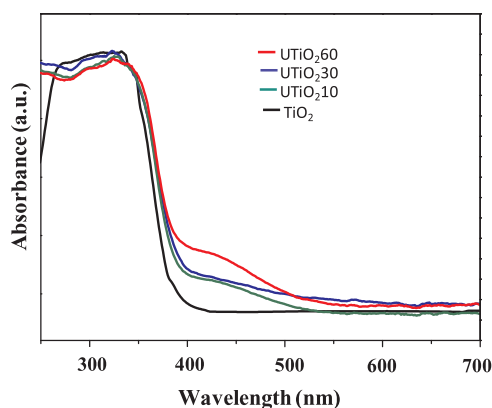
Fig. 1. DRS spectrum of TiO_2 nanoparticles modified with urea at different urea: TiO_2 ratios (%wt).
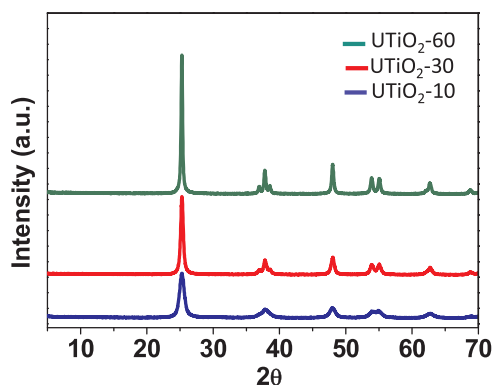

Fig. 2. X-ray Diffractogram of TiO_2 nanoparticles modified with urea.

substitutional N-doping, which may depend on the synthesis procedure. For instance, the authors suggested that sol-gel synthesis leads only to the interstitial N-doping when nitrogen precursors such as NH_4Cl, urea or NH_3 were used [25,26]. Both interstitial and substitutional N-doping may induce nitrogen-mid-gap levels responsible for visible light absorption.

On the other hand, Mitoraj and Kisch [27,28] claimed that visible-light absorbing TiO_2 prepared by mechanochemical method and using urea as nitrogen source really did not show N-doping but its visible light absorption was probably due to the formation of urea thermolysis by-products such as melem, melon or polytriazine shell often known as g-C_3N_4. Precisely, g-C_3N_4 structures with visible light absorption as melon, have been recently described as very promising photocatalysts, especially in H_2 production [29–31].

Regarding the using of visible-light active nitrogen modified TiO_2 as self-cleaning material, few studies can be found in the literature. For instance, Irie et al. [32] and Prenkumar [33] found for the first time that thin films of "N-doped" TiO_2 deposited on SiO_2 coated glass and prepared by sputtering showed high visible light induced super hydrophilicity. Both authors suggested that visible light activity was caused by band gap narrowing following the theory described by Asahi et al [21].

Kimiagar and Mohammadizadeh [34] reported the synthesis via sol-gel of N-doped TiO_2 nanoparticles from urea as nitrogen precursor and then their immobilization in glass. Photocatalytic activity of these materials was evaluated by UV-photo-degradation of methylene blue (MB) on their surface finding high discoloration activities. Vaiano et al. [35] prepared ceramic tiles functionalized with N-doped TiO_2, urea as N-doping precursor and annealed at 550 °C. MB was also used as target but in aqueous media irradiating with UV and blue light. Results demonstrated that upon UV-irradiation, MB was rapidly degraded while upon blue light, photocatalytic activity was minor. Finally, in 2017, Kusano et al. [36] reported the preparation of N-doped TiO_2 thin films on Si (100) substrates.

Some studies have reported that polymeric substrates can be used as supports of TiO_2 nanoparticles and then evaluated as self-cleaning
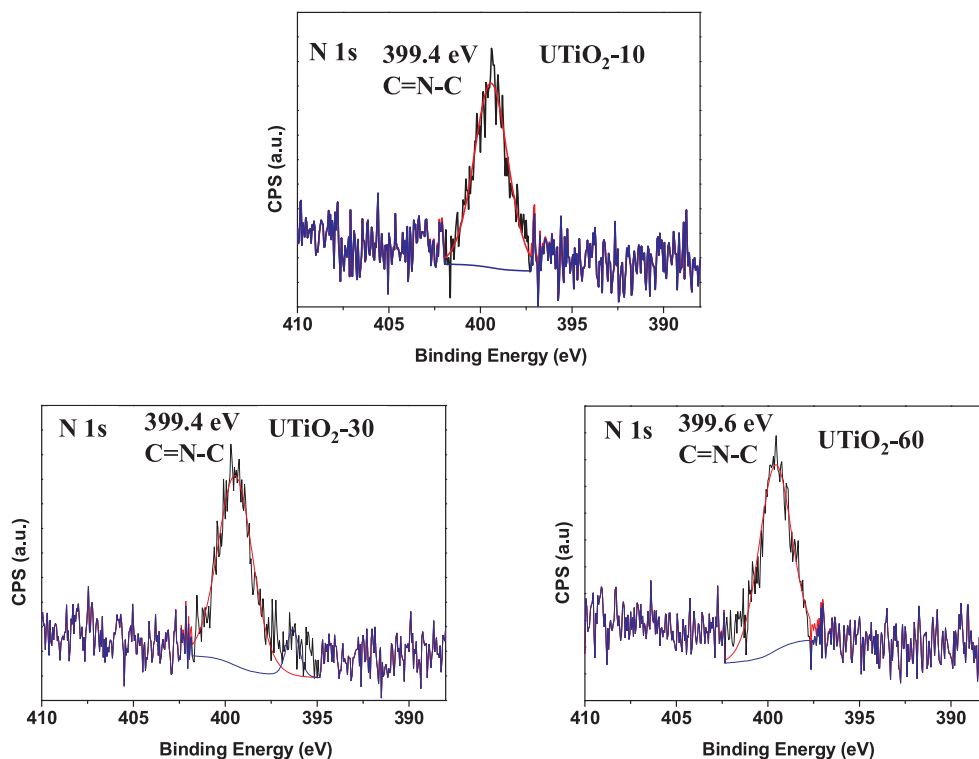

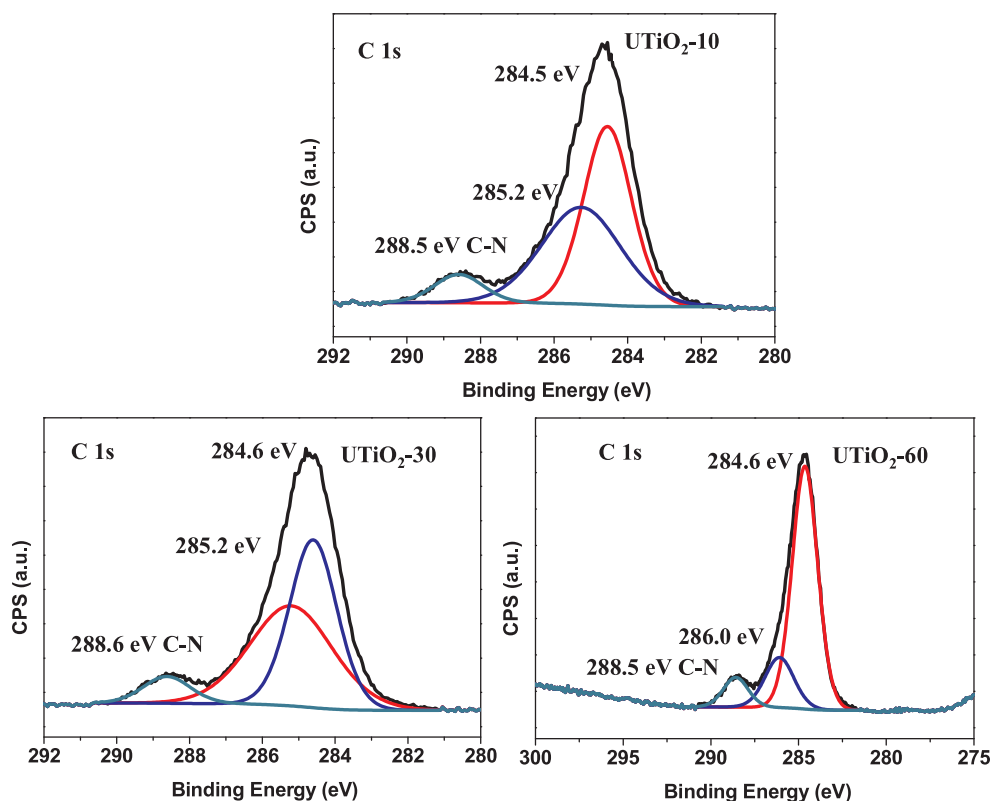**Fig. 3.** XPS deconvoluted N 1 s spectra of urea-modified TiO_2 nanoparticles.

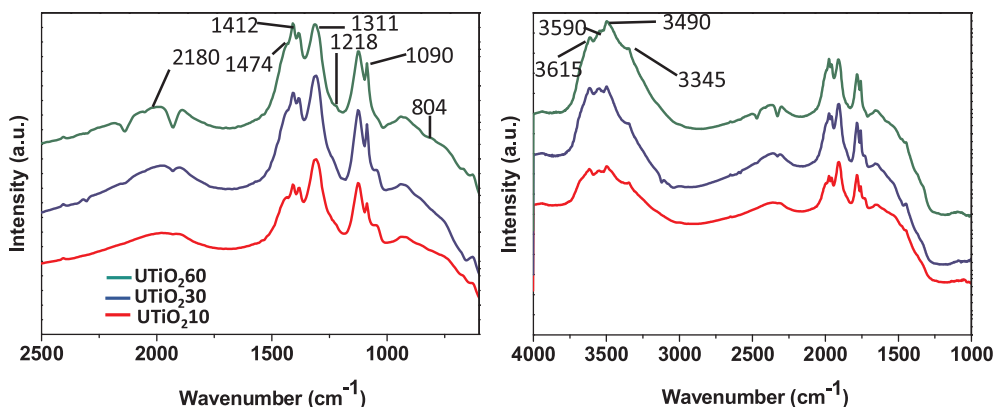**Fig. 4.** XPS deconvoluted C1 s spectra of urea-modified TiO_2 nanoparticles.

Fig. 5. Diffuse reflectance infrared fourier transform spectroscopy (DRIFTS) of TiO_2 nanoparticles modified with urea at different urea: TiO_2 ratios (%wt).

surfaces [37–40]. An interesting biopolymer, chitosan (QS), a natural polymer with hydrophilicity, biocompatibility, biodegradability and nontoxic properties [41] has been explored as a substrate to immobilize TiO_2 nanoparticles. Nevertheless, the most part of studies have been addressed to the removal of waterborne pollutants such as organic dyes, bacteria inactivation, and as wound dressing material [42–46]. Recently, Rengifo-Herrera et al. [47] published a study about the using of chitosan films containing visible-light active TiO_2 nanoparticles modified with tungstophosphoric acid (TPA). The photocatalytic activity in solid/gas interfaces was evaluated by malachite green degradation upon different wavelengths.

To our knowledge, there are few studies reporting chitosan films containing heterojunctions of melon/TiO_2 with self-cleaning capacity photoinduced with visible light. Herein, it is reported for the first time the synthesis by sol-gel method and multi-technique characterization of visible light active TiO_2 nanoparticles modified with urea (at different weight percentage) and their immobilization in chitosan films, a

biopolymer with interesting features such as biocompatibility, biodegradability and nontoxic properties. Photo-induced self-cleaning capacity of films was studied by degradation of malachite green in solid/gas interfaces and followed through DRS-UV–vis and ATR-FTIR irradiating upon three different wavelengths including UV-A + visible (320–800 nm) and two kinds of visible light portions (450–800 nm and 590–800 nm). This separation was done considering that UV-A light excites only anatase TiO_2 nanoparticles. Visible light with wavelengths comprised between 450–800 nm would be able to excite only urea modified anatase TiO_2 nanoparticles and malachite green molecules and finally, light irradiation at 590–800 nm would be only able to excite malachite green molecules. Thus, is feasible to study the different photochemical events taking place in films stained with malachite green dye and determinate the several reactions responsible of malachite green stains photo-fading.
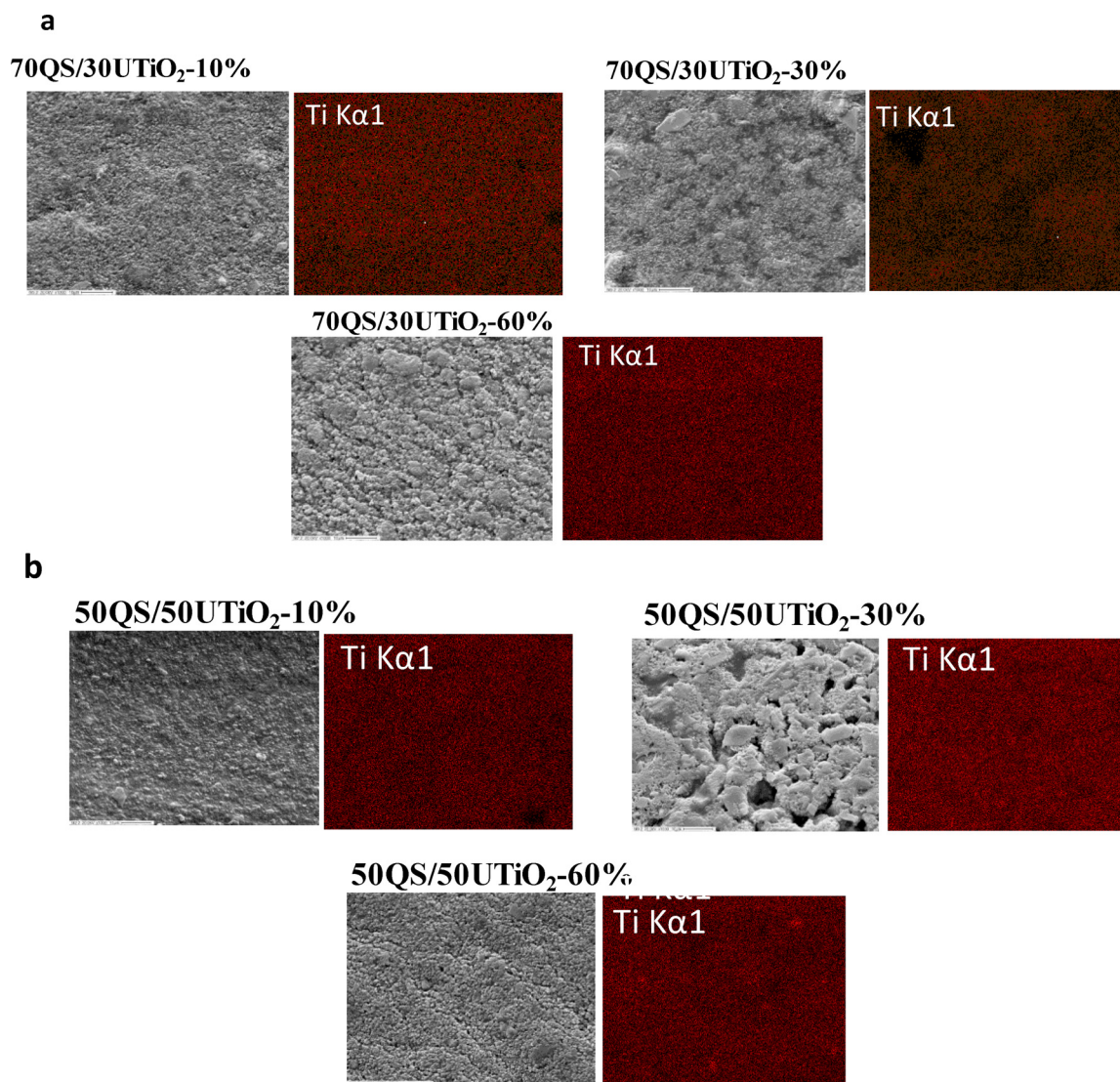
a

70QS/30UTiO$_2$-10%

Ti Kα1

70QS/30UTiO$_2$-30%

Ti Kα1

70QS/30UTiO$_2$-60%

Ti Kα1

b

50QS/50UTiO$_2$-10%

Ti Kα1

50QS/50UTiO$_2$-30%

Ti Kα1

50QS/50UTiO$_2$-60%

Ti Kα1

Fig. 6. SEM micrographs at 1000x of chitosan films (with different urea ratios, 10, 30 and 60% (wt)). EDS mapping of Ti line Kα1. (a) 70QS/30UTiO$_2$ and (b) 50QS/50UTiO$_2$ films.
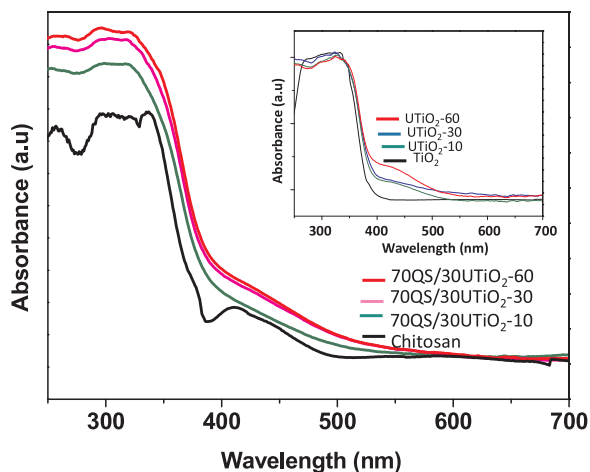

Fig. 7. DRS spectrum of functionalized chitosan films (70QS/30UTiO$_2$-X) containing TiO$_2$ nanoparticles modified with urea at different urea: TiO$_2$ ratios (%wt). Insert shows the DRS spectrum of UTiO$_2$ nanoparticles.

2. Experimental section

2.1. Materials

The chemical substances used to synthesize the TiO$_2$-based samples and perform the photobleaching tests were: titanium tetraisopropoxide (99%, Sigma-Aldrich), urea (99%, Sigma-Aldrich), malachite green oxalate (99%, Sigma-Aldrich), ethanol (Merck, absolute grade), HCl (37%, Carlo Erba), P-25 TiO$_2$ nano-powders (Evonik), glacial acetic acid (Carlo Erba). All chemicals were used as received.

2.2. Nanoparticle and film synthesis

2.2.1. Synthesis of TiO$_2$ nanoparticles modified with urea

The synthesis was carried out following this method:

Titanium isopropoxide was mixed with absolute ethanol and stirred under N$_2$ atmosphere at room temperature. Then, an urea-ethanol solution (urea content 10, 30 and 60 wt%) was added to the titanium isopropoxide solution simultaneously with a suitable volume of HCl 0.28 M and stirred vigorously for 2 h.

The gel was dried in a beaker at room temperature and then, the solids were ground into powder and thermally treated at 400 °C for 1 h
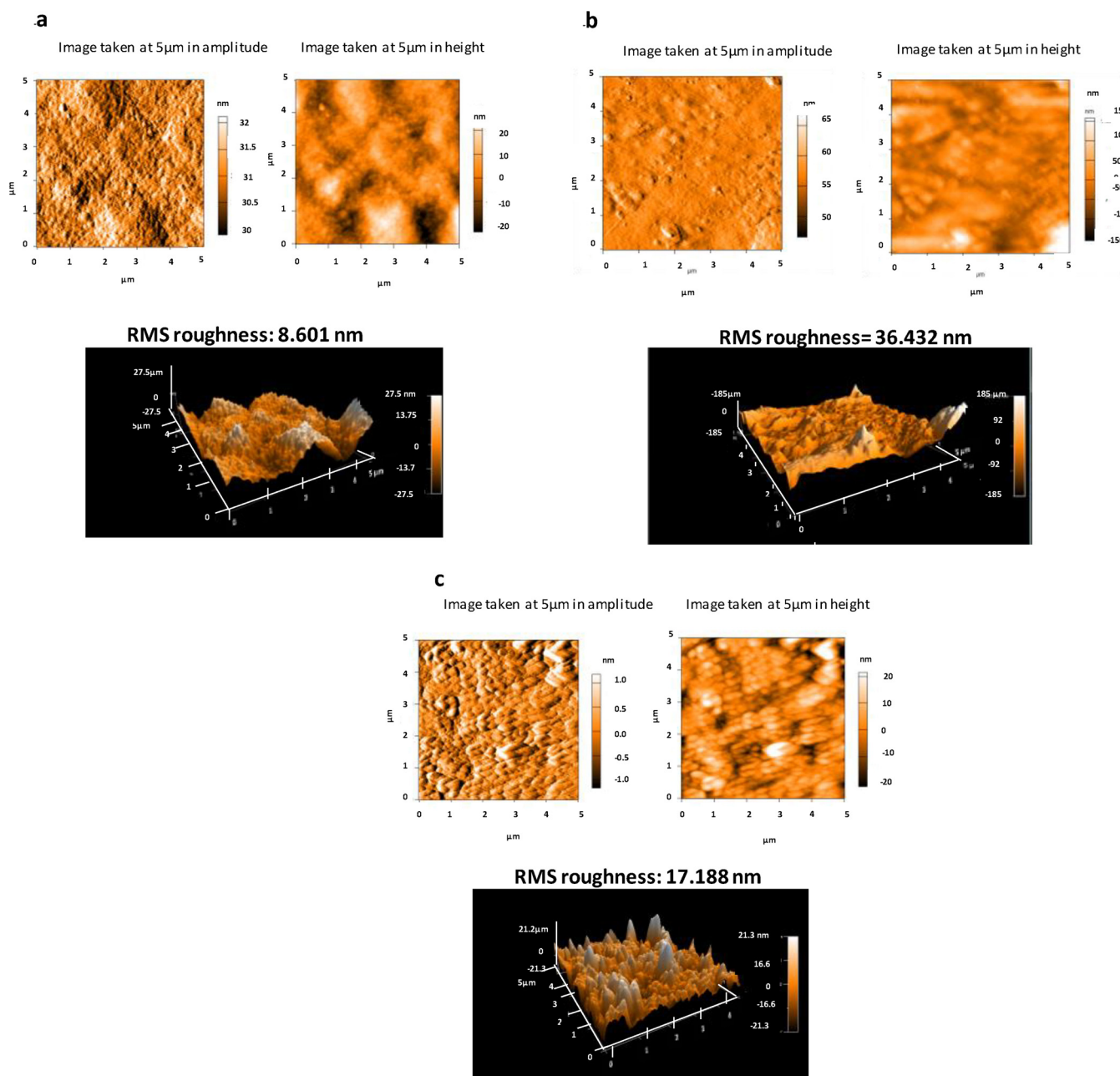
a

Image taken at 5μm in amplitude   Image taken at 5μm in height

RMS roughness: 8.601 nm

b

Image taken at 5μm in amplitude   Image taken at 5μm in height

RMS roughness= 36.432 nm

c

Image taken at 5μm in amplitude   Image taken at 5μm in height

RMS roughness: 17.188 nm

Fig. 8. Atomic force microscopy (AFM) images in noncontact mode and surface morphology in three dimensions of 70QS/30UTiO$_2$-X films where X represents the urea: TiO$_2$ ratio in %wt.

using a heating ramp of 5 °C per minute. Finally, the obtained materials were washed using an ultrasound bath for 3 min in Milli-Q water (this operation was repeated three times), filtered and dried at 60 °C for 24 h. Synthesized materials were labelled as UTiO$_2$-10, UTiO$_2$-30 and UTiO$_2$-60.

2.2.2. Synthesis of chitosan/UTiO$_2$ and chitosan/P-25 films

A chitosan solution (QS) 1.0% (w/w) was prepared by solubilization in 1.0% (v/v) acetic acid solution as was described by Lamarra et al. in previous work [48]. Different amounts of UTiO$_2$ or P-25 nanoparticles were dispersed in the chitosan solution to obtain chitosan/nanoparticles ratios of 70:30 and 50:50 (%wt). The functionalized films were prepared by casting and drying at 37 °C until reaching a constant weight. Hereinafter, the synthetized films will be named as 70QS/30UTiO$_2$-X or 50QS/50UTiO$_2$-X (where X exhibits the urea %wt added on TiO$_2$ nanoparticles).

2.2.3. Nanoparticles and chitosan films characterization

A multi-technique characterization was performed on both urea-modified TiO$_2$ nanoparticles and chitosan films. TiO$_2$ nanoparticles were characterized by diffuse reflectance spectroscopy (DRS), diffuse reflectance Fourier transform infrared spectroscopy (DRIFTS), X-ray photoelectron spectroscopy (XPS), X-ray diffraction (XRD). Furthermore, nitrogen and carbon content was also measured in urea modified TiO$_2$ nanoparticles. Functionalized films characterization was performed by DRS, scanning electronic microscopy coupled with energy dispersive X-ray spectroscopy (SEM-EDS), atomic force microscopy (AFM) (Further details in Supplementary information).

2.3. Photobleaching experiments

Photobleaching experiments were carried out following the methodology reported by Rengifo-Herrera et al. (Further details in
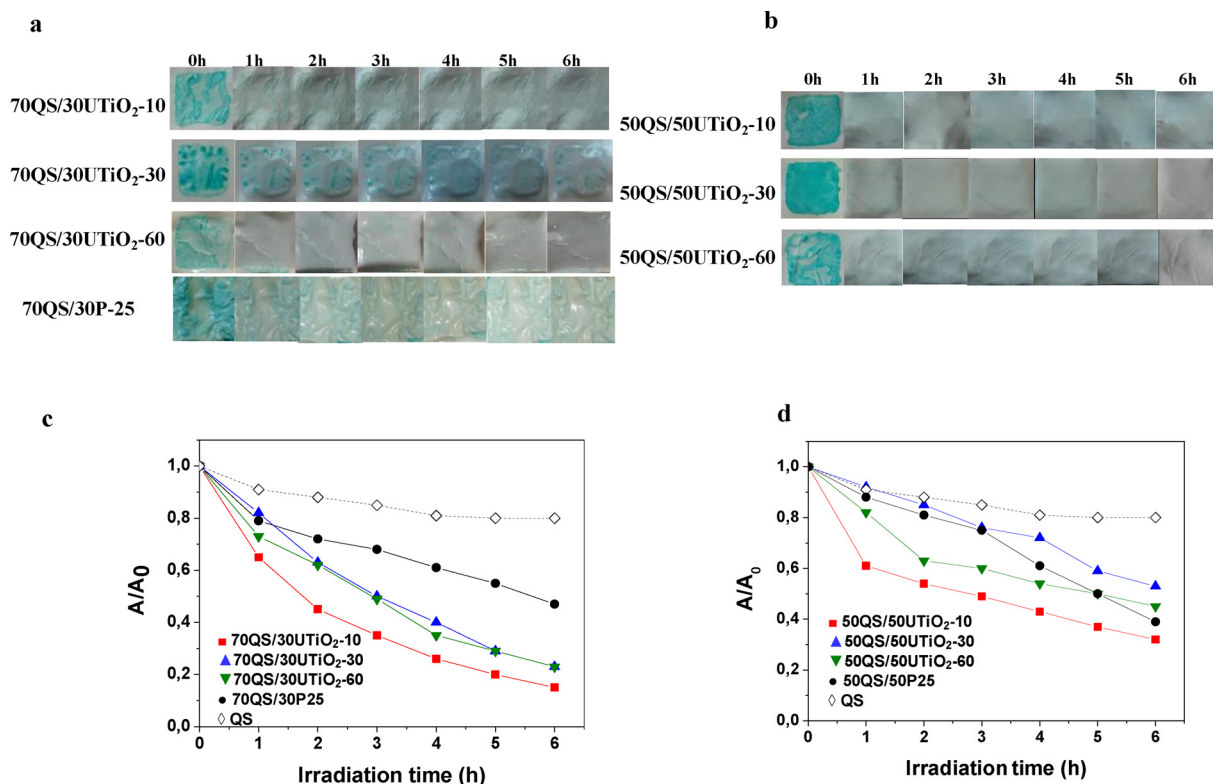
Fig. 9. Photobleaching of malachite green stains (10^{-4} mol L^{-1}) during 6 h on chitosan films containing UTiO$_2$ nanoparticles at different urea: TiO$_2$ ratios upon UV-A + visible (320–800 nm) irradiation using a 200 W Xe-Arc lamp. UV-A irradiance was around 35 W m^{-2}. (a) 70QS/30UTiO$_2$-X films. (b) 50QS/50UTiO$_2$-X films (c) plot of normalized absorbance at 624 nm vs irradiation time for 70QS/30UTiO$_2$-X films (d) plot of normalized absorbance vs irradiation time for 50QS/50UTiO$_2$-X film (For interpretation of the references to colour in this figure legend, the reader is referred to the web version of this article).

Supplementary information). In addition, this time a plot of normalized absorbance of malachite green dye at 624 nm vs irradiation time was obtained following the methodologies reported in the literature [49,50].

Reusing experiments were also performed. Three reusing cycles of 6 h of irradiation were carried out using the same film and then characterization by SEM and AFM was achieved.

3. Results

3.1. Characterization of TiO$_2$ nanoparticles modified with urea

Fig. 1 shows that all TiO$_2$ studied nanoparticles studied exhibited the typical UV-absorption of TiO$_2$ below 400 nm [51]. However, urea modified nanoparticles revealed a visible light absorption at wavelengths comprised between 400 and 500 nm, a common feature of urea-modified TiO$_2$ nanoparticles [52–54]. Visible light absorption increased by raising the urea content. XRD diffraction patterns (Fig. 2) showed the presence of peaks at 2θ around 24.9° (1 0 1), 37.9° (0 0 4), 47.8° (2 0 0) and 54.3° in all the nanoparticles samples attributed exclusively to anatase TiO$_2$ [55,56].

XPS spectra of deconvoluted N 1 s (Fig. 3) and C 1 s (Fig. 4) peaks revealed signals at 399.0 and 288.6 eV respectively (Signals of C 1 s at 284.0 and 285.0 eV were attributed to adventitious carbon). DRIFT spectra (Fig. 5) showed bands at 3345, 3490, 3590 and 3615 cm^{-1} which could be assigned to N−H bonds. Other group of signals were detected at 1589, 1462, 1392 and 1356 cm^{-1} and corresponding to N═C and N−C bonds respectively.

Moreover, elemental analysis measurements (see Table 1S in Supplementary information) did not show measurable nitrogen amounts in UTiO$_2$-10 and UTiO$_2$-30 nanoparticles while in UTiO$_2$-60 nitrogen-concentration was around 0.1%. In contrast, C content was

detectable in concentrations of 0.1, 0.2 and 0.4% for samples UTiO$_2$-10, UTiO$_2$-30 and UTiO$_2$-60 respectively.

3.2. Characterization of chitosan films containing TiO$_2$ nanoparticles modified with urea

SEM micrographs (Fig. 6) show a rough surface in all films with the concomitant presence of urea-modified TiO$_2$ nanoparticles. Furthermore, EDS mapping following the line Kα1 of Ti revealed that UTiO$_2$ nanoparticles were homogeneously dispersed on the film.

DRS spectra of different films containing 30% of UTiO$_2$ nanoparticles (%wt) (Fig. 7) (70QS/30UTiO$_2$), exhibited UV light absorption corresponding to chitosan. However, it was also observed the presence of a light absorption shoulder between 400 and 500 nm which could be linked to the presence of UTiO$_2$ nanoparticles. Similar features were found to 50QS/50UTiO$_2$ films.

AFM measurements were also performed within a scanned area of 5 × 5 μm^2. Chitosan films showed a smooth surface and low RMS roughness (Fig. 8a). In contrast, 70QS/30UTiO$_2$-10 and 50QS/50UTiO$_2$-10 films (Fig. 8b and 8c) exhibited a surface with high roughness which was confirmed by RMS roughness data. These data revealed that presence of UTiO$_2$ nanoparticles on chitosan films changed the polymer surface properties.

3.3. Photobleaching of malachite green stains upon different wavelengths

QS/UTiO$_2$ films stained with malachite green ethanolic solution were irradiated up to 6 h upon different wavelengths. Fig. 9 shows experiments carried out upon UV-A + visible light irradiation (320–800 nm). Dark essays on QS/UTiO$_2$ did not exhibit dye bleaching (Data not shown). However, Fig. 9a shows experiments with 70QS/30UTiO$_2$ films which revealed an interesting photobleaching activity.
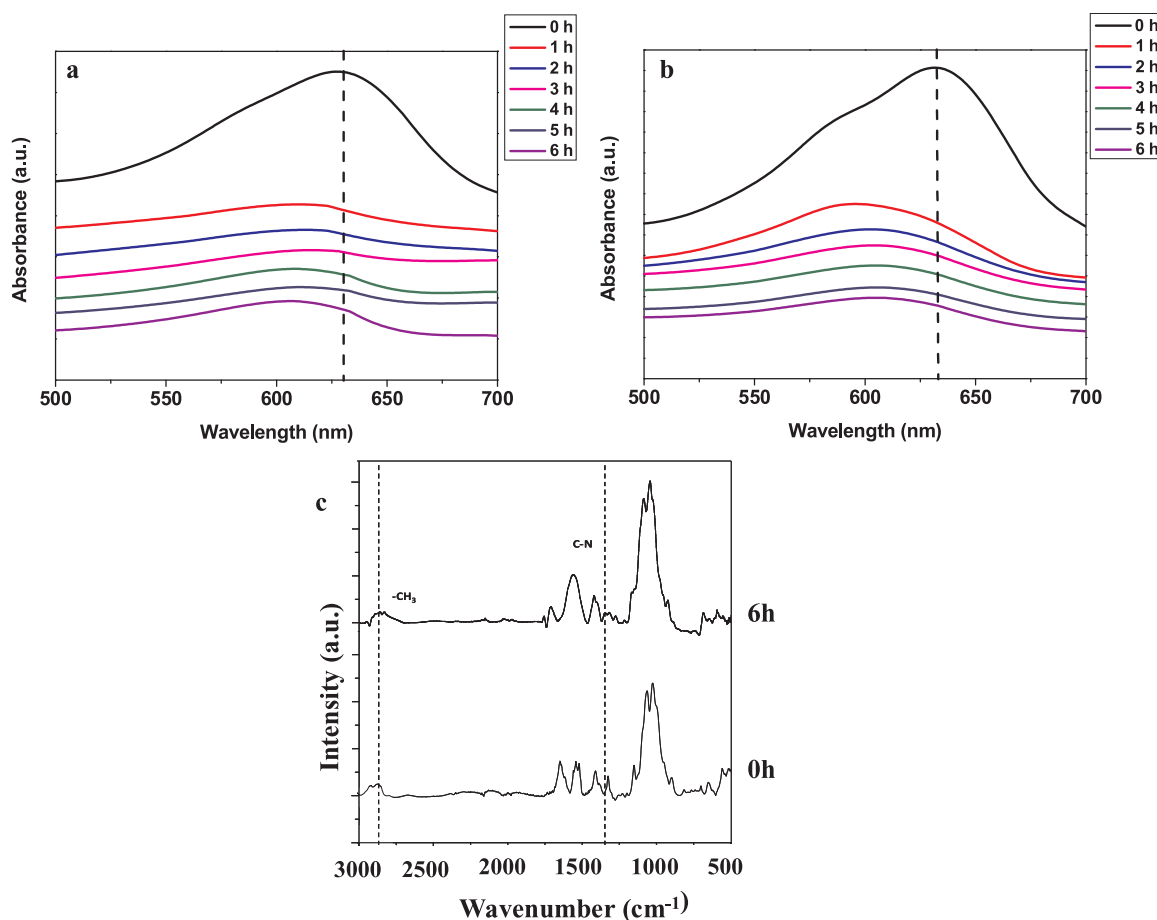
Fig. 10. Evolution of malachite green main light band absorption at 624 nm during UV−A + Visible light irradiation in (a) 70QS/30UTiO$_2$-10 film. (b) 50QS/50UTiO$_2$-10 film. (c) Attenuated total reflection Malachite green IR peaks monitored by Fourier transform infrared spectroscopy (ATR-FTIR) spectrum in 70QS/30UTiO$_2$-10 film. Subtraction of chitosan and UTiO$_2$ IR bands were achieved. (For interpretation of the references to colour in this figure legend, the reader is referred to the web version of this article).

The plot of normalized absorbance vs irradiation time (Fig. 9c) showed that especially those films with UTiO$_2$ nanoparticles prepared with 10% (%wt) of urea (70QS/30UTiO$_2$-10) exhibited the best photobleaching activity. In addition, films 50QS/50UTiO$_2$ (Fig. 9b and 9d) showed a similar behavior. When films with the highest photobleaching activity were compared with those of chitosan containing P-25 nanoparticles, this latter showed a lower photo-activity while chitosan films (QS) without nanoparticles exhibited a very low photobleaching activity.

Malachite green absorption spectrum was followed by DRS at different irradiation times for the films 70QS/30UTiO$_2$-10 and 50QS/50UTiO$_2$-10 (Fig. 10a and b). Two features were identified: (*i*) the intensity of the main absorption band of malachite green (λ_{max} = 624 nm) decreased by rising the irradiation time and in addition, (*ii*) this band underwent a blue shifting (593 nm) caused probably for N-demethylation of malachite green [57,58]. Unsymmetrical and symmetrical bi-demethylated malachite green molecules absorb light at 592 and 593 nm respectively [59], thus during UV–vis light irradiation, modified UTiO$_2$ could induce the formation of these byproducts.

ATR-FTIR measurements on films 70QS/30UTiO$_2$-10 (Fig. 10c) following IR signals of malachite green dye showed that after 6 h of UV + visible irradiation, those bands at 2800 and 1375 cm^{-1} corresponding to bending of C–H and C–N bonds respectively of −CH$_3$ groups underwent a strong intensity reduction.

On the other hand, under visible light irradiation (450–800 nm), where both urea-modified TiO$_2$ and malachite green can absorb light, pictures revealed a significant dye photobleaching (Figure S1 supplementary material) also on 70QS/30UTiO$_2$-10 and 50QS/50UTiO$_2$-10

films. Fig. 11a shows that malachite green dye underwent a strong photobleaching on both films even higher than films containing Degussa P-25. DRS spectra recorded during the irradiation time Fig. 11b and 11c) revealed that malachite green underwent N-demethylation process caused probably by the attack of photo-induced hydroxyl radicals or valence band holes on UTiO$_2$ nanoparticles. However, ATR-FTIR spectrum (Fig. 11d) of 70QS/30UTiO$_2$-10 film stained with malachite green showed that peaks at 2800 cm^{-1} corresponding to −CH$_3$ groups of dye were not strongly affected. In contrast, a new band localized at 1620 cm^{-1} appeared after 6 h of visible light irradiation. This band could be assigned to -C = O vibrations of ketones. Previous studies have claimed that malachite green molecule could exhibit oxidative attack from singlet oxygen (^{1}O$_2$) leading to the production of benzophenones [60,61]. Thus, this -C = O vibrations could be assigned to the presence of these chemical substances.

Those experiments carried out under visible light (590–800 nm) on films 70QS/30UTiO$_2$-10 and 50QS/50UTiO$_2$-10 where only the malachite green molecule can absorb light, revealed a weak photobleaching of dye stains (Fig. 12a and S2 of supplementary information). DRS spectra recorded on film 70QS/30UTiO$_2$-10 (Fig. 12b) showed a slight blue-shifting of the dye main absorption band. ATR-FTIR spectrum of the same film (Fig. 12c) revealed also the presence of –C = O band at 1620 cm^{-1} coming from benzophenones formation.

3.4. Reusing experiments

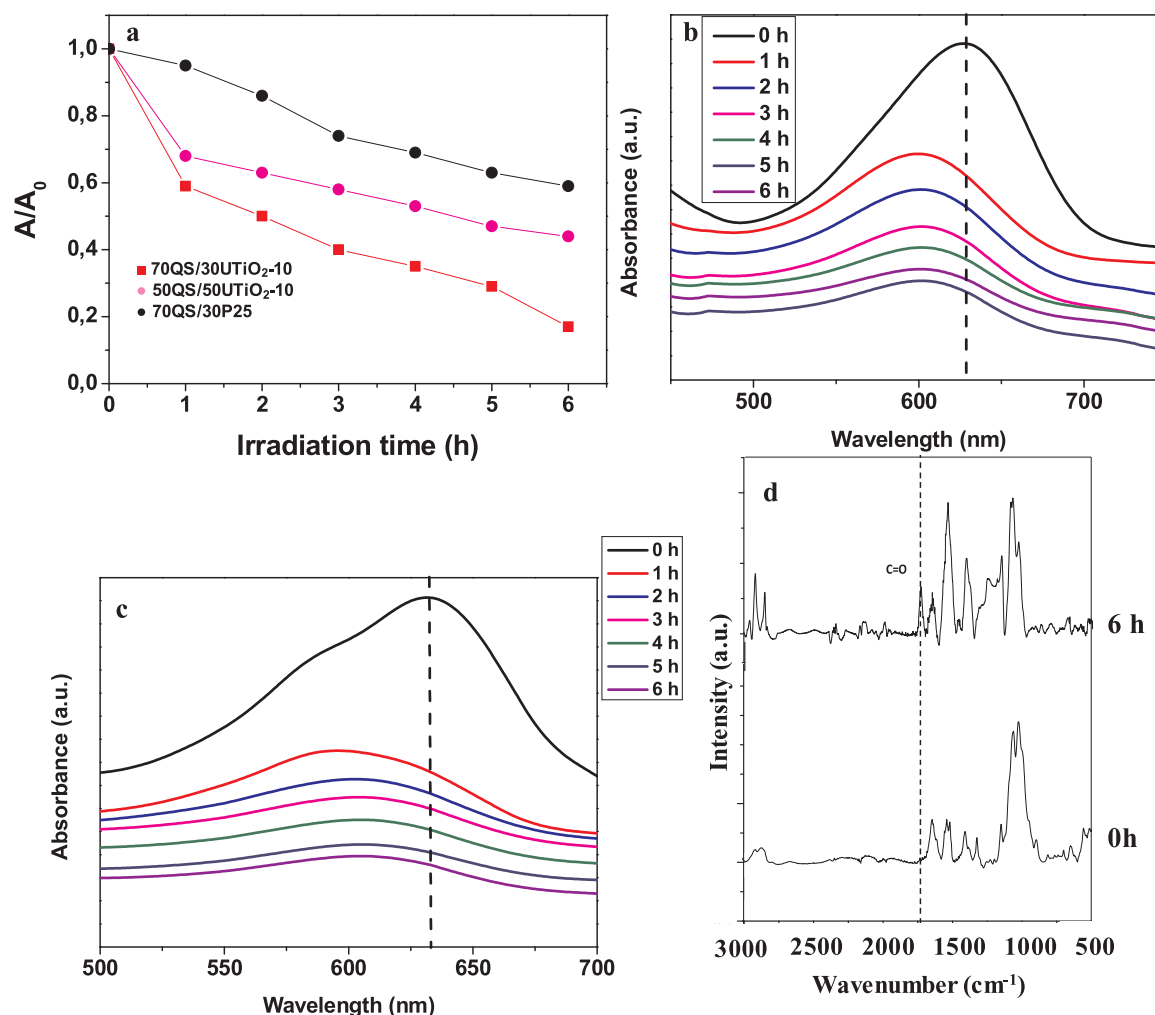The film 70QS/30UTiO$_2$-10 was tested in reusing experiments. This

Fig. 11. (a) Photobleaching of malachite green stains (10^{-4} mol L^{-1}) by following the normalized absorbance at 624 nm vs irradiation time in 70QS/30UTiO$_2$-10, 50QS/50UTiO$_2$-10 and 70QS/30P25 films upon visible irradiation (450–800 nm) using a 200 W Xe-Arc lamp. Malachite green main absorption band at 624 nm monitored during Visible light irradiation in (b) 70QS/30UTiO$_2$-10 film. (c) 50QS/50UTiO$_2$-10 film. (d) Malachite green IR peaks followed by attenuated total reflection Fourier transform infrared (ATR-FTIR) spectrum on 70QS/30UTiO$_2$-10 film. Subtraction of chitosan and UTiO$_2$ IR bands were performed. (For interpretation of the references to colour in this figure legend, the reader is referred to the web version of this article).

was exposed to 18 h (3 cycles of 6 h) of UV + Visible light irradiation (320–800 nm) without the significant loosing of its photobleaching activity (Fig. 13). However, light irradiation led to the changes on the film surface since SEM micrographs showed some erosion, fact confirmed by AFM measurements (Fig. 14). AFM images also evidenced that after 18 h of continuous UV-A + visible light irradiation, the RMS roughness increased from 36.432 nm to 40.264 nm. This fact could be also related to surface erosion.

4. Discussion

Historically, visible light absorption of urea-modified TiO$_2$ nanoparticles prepared by sol-gel method and annealing at either 450 and 600 °C has often been linked to XPS N 1 s signals at 399 eV corresponding to N-doping by formation of N-Ti-O bonds [19] and N 1 s signals at 396 eV attributed to Ti-*N*-O bonds [62]. However, as it was already described, Mitoraj and Kisch [27,28] proposed for the first time that visible light absorption of TiO$_2$ modified with urea should be related to the presence of urea thermolysis byproducts such as melon (a yellowish substance). It is well known that urea undergoes thermolysis reactions on TiO$_2$ starting at temperatures above its melting point (133 °C) leading to the production of gaseous ammonia and isocyanic acid. This latter is highly reactive in presence of hydroxyl groups-

contained in solid surfaces and at temperatures oscillating between 190 and 250 °C could be converted into cyanuric acid which would keep reacting to produce heterocyclic condensed byproducts such as ammelide, ammeline, melam, melem and melamine [27,28,63–65]. All these chemical substances are white, and it could not be responsible for visible light absorption (Figure S3 Supplementary information).

In 2011, Zou et al. [66] claimed that the conversion of urea into graphitic carbon nitride (known also as g-C$_3$N$_4$) over TiO$_2$ at 300 °C was feasible. The presence of g-C$_3$N$_4$ could be linked to the visible light absorption experimented on these TiO$_2$ nanoparticles.

g-C$_3$N$_4$ or graphitic carbon nitride are polymer-like materials with different properties used in several applications such as Friedel-Craft reactions, cyclization of functional nitrides and alkynes and recently some of these materials such as melon (which is a heptazine ring) have been described as photocatalyst in H$_2$ production [29,31,67–69].

Graphitic carbon nitride shows IR bands in region of 1200-1650 cm^{-1} from the formation of extended networks of C–N = C bonds [70]. On the other hand, melon exhibits IR signals at 1253 cm^{-1} (ν_{C-N}) 1318 cm^{-1} (ν_{C-N}), 1411 cm^{-1} (δ_{N-H}), 1477 cm^{-1} (ν-ring), 1633 cm^{-1} (δ_{N-H}) and 3150 cm^{-1} (ν_{N-H}) and the typical IR band linked to heptazine ring at 801 cm^{-1} [71–73]. N and C 1 s XPS spectra of melon show signals at 398.8 and 288.4 eV which could be attributed to C = N–C bonds [73,74]. On the other hand, as it was mentioned before, melon is
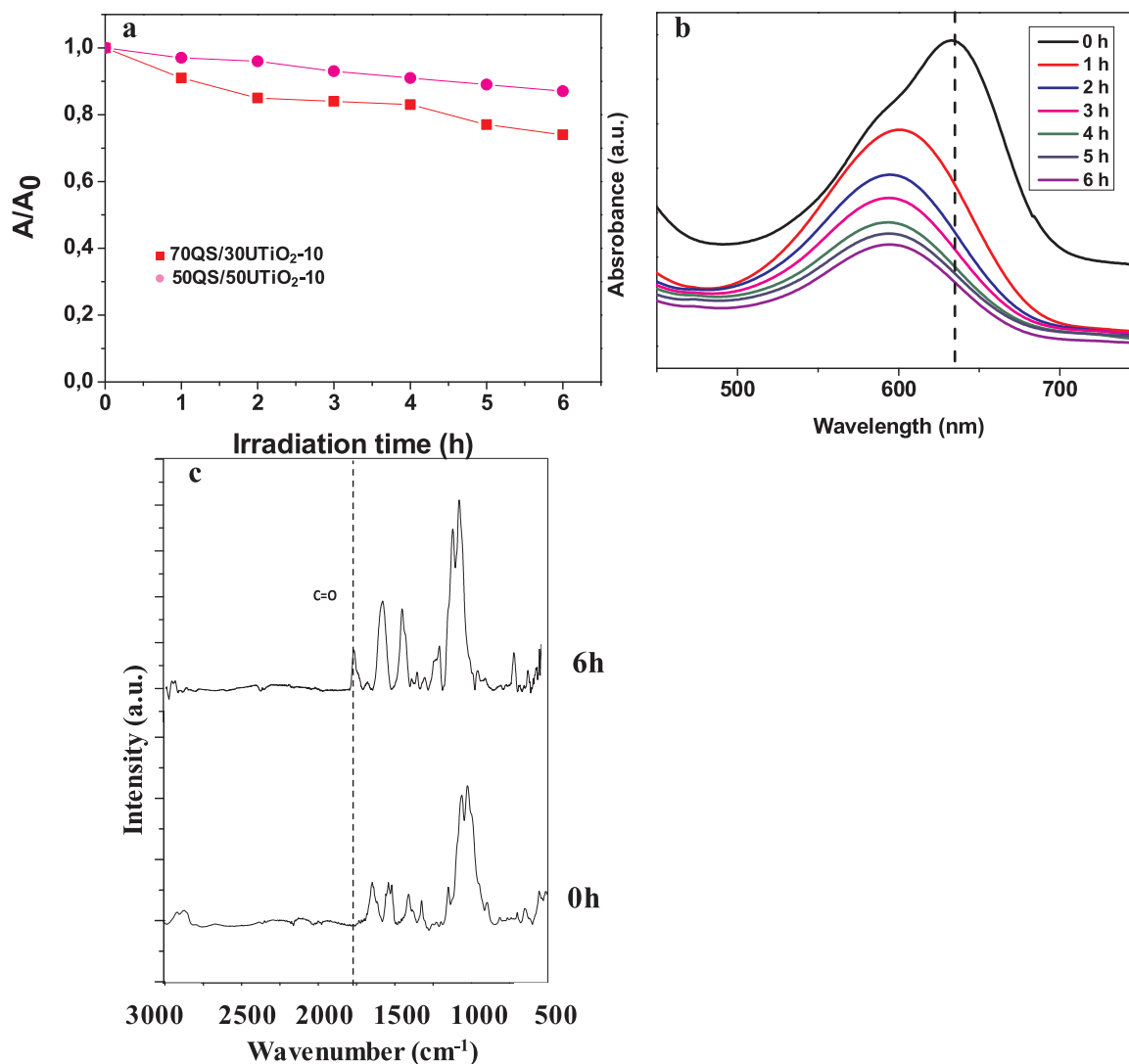
Fig. 12. (a) Photobleaching of malachite green stains (10^{-4} mol L^{-1}) on 70QS/30UTiO$_2$-10, 50QS/50UTiO$_2$-10 films upon visible irradiation (590–800 nm) using a 200 W Xe-Arc lamp following the normalized absorbance at 624 nm vs irradiation time. (b) Evolution of dye main band absorption at 624 nm in 70QS/30UTiO$_2$-10 film (c) malachite green main IR peaks by total reflection Fourier transform infrared spectroscopy (ATR-FTIR) during visible light irradiation in 70QS/30UTiO$_2$-10 film. Subtraction of chitosan and UTiO$_2$ IR bands were achieved. (For interpretation of the references to colour in this figure legend, the reader is referred to the web version of this article).

a yellow substance and exhibits a band gap energy around 2.7 eV which allows absorbing light at wavelengths below 500 nm [73].

Mitoraj and Kisch [27,28] suggested that the yellowish color observed in TiO$_2$ nanoparticles modified with urea could be due to the presence of melon since authors found the same N 1 s XPS and FTIR signals mentioned above.

With all this information, we also suggest that these TiO$_2$ nanoparticles modified with urea could contain melon on the titania surface since XPS, DRIFT-IR, and DRS studies evidenced signals which could be attributed to the presence of this compound. Thus, a heterojunction between TiO$_2$ and melon could be possible since recently, g-C$_3$N$_4$ materials such as melon have been catalogued as semiconductors with a band gap energy around 2.7 eV and conduction band and valence band potentials of -1.3 and +1.4 V (vs NHE) respectively [31] making thermodynamically possible transfer of photo-excited electrons from the melon CB to TiO$_2$ CB (Fig. 15).

Photo-bleaching activity revealed that these functionalized films showed UV and visible induced photocatalytic processes. It is important to highlight that apparently those films containing visible light absorbing TiO$_2$ nanoparticles modified with low urea concentrations

(10% wt/wt) exhibited a high photocatalytic activity. Although nitrogen content was only detected by elemental analysis in nanoparticles synthesized with highest urea addition (60% w/w), it is possible to suggest that TiO$_2$ nanoparticles prepared with high urea loads (30 and 60% w/w) would produce high content of urea thermal byproducts affecting negatively their photocatalytic activity. Previously, some studies had claimed that in synthesis of modified urea TiO$_2$ nanoparticles either by mechanochemical and sol-gel processes, rising the urea concentration added during the synthesis, the photocatalytic activity decreases, since high amounts of thermolysis urea byproducts could be induced. High accumulation of these chemical substances on TiO$_2$ surfaces could produce a detrimental effect on the photocatalytic activity [75,76]. On the other hand, increasing the concentration of urea modified TiO$_2$ nanoparticles on chitosan films did not enhance or decrease markedly the observed photocatalytic activity.

UV absorption of urea-modified TiO$_2$ and P-25 seems to be the main process responsible for dye photobleaching on chitosan films. Either photo-induced VB holes or ·OH radicals should be responsible for the photo-induced activity. This oxidative attack should lead to the N-de-methylation process on malachite green molecules yielding the blue-
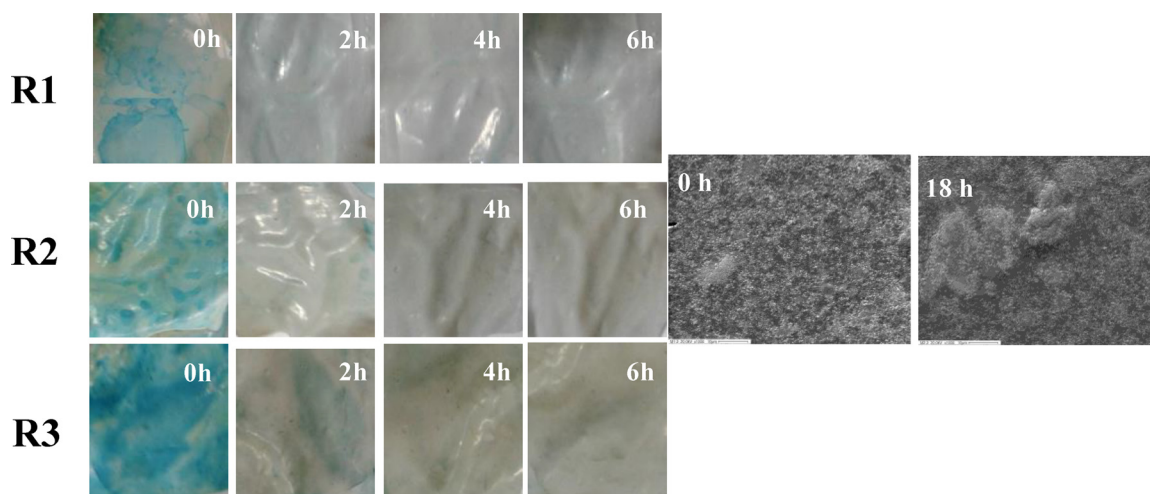
Fig. 13. Reusing experiments measuring malachite green photo-bleaching on 70QS/30UTiO$_2$-10 film during 3 cycles of 6 h upon UV-A + visible light irradiation. SEM micrographs before and after of photo-irradiated experiments. UV-A irradiance was around 35 W m^{-2}. (For interpretation of the references to colour in this figure legend, the reader is referred to the web version of this article).
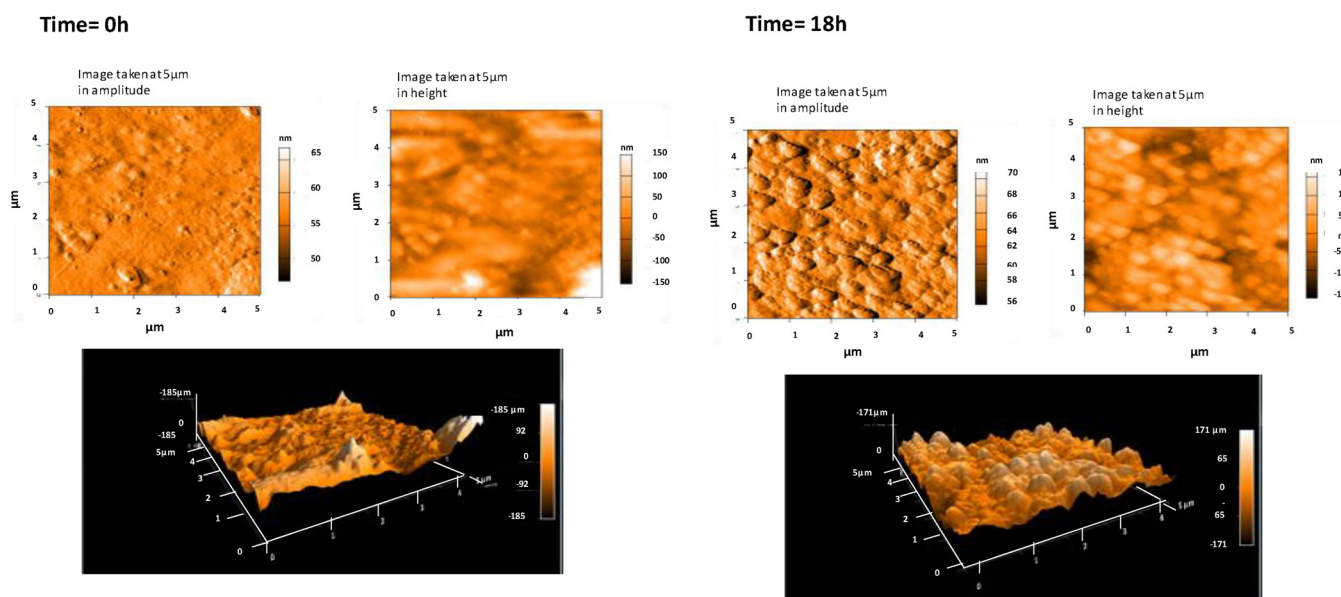

Fig. 14. Atomic force microscopy (AFM) images in noncontact mode and surface morphology in three dimensions of 70QS/30UTiO$_2$-10 film before and after 3 cycles of 6 h upon UV-A + visible light irradiation. UV-A irradiance was around 35 W m^{-2}.

shifting of their main absorption band. It is well known that waterborne malachite green undergoes N-demethylation process under UV-induced photocatalytic reactions over TiO$_2$ [57,58]. Unsymmetrical and symmetrical di-demethylated byproducts absorb light at 593 and 592 nm respectively [59]. DRS spectra showed that main dye absorption band at 624 nm underwent shifting towards 592 nm, thus it should be possible that photoinduced VB holes or hydroxyl radicals photoinduced on UTiO$_2$ nanoparticles attack the N atom of malachite green leading to the N-demethylation of dye molecule (Fig. 16).

In contrast, under visible light (450–800 nm and 590–800 nm) there was a minor photo-bleaching effect and a slight dye band absorption blue shifting. Moreover, ATR-FTIR spectra showed the presence of a ketonic malachite green oxidative byproduct. Duxbury [60] and Kuramto and Kitao [61] have mentioned that malachite green molecule is susceptible to form benzophenones (4-dimethylaminobenzophenone and 4-aminobenzophenone) by attack of singlet oxygen on the central carbon of dye molecule.

In this case, three routes could be responsible of the formation of benzophenones (Fig. 16): the first route may involve dye photo-excited

states induced by absorption at wavelengths close to the main absorption band of malachite green (around 624 nm). Excited states of dye could react with molecular oxygen through energy transfer reactions leading to the production of ^{1}O$_2$. The second one may involve photochemical reactions where melon and TiO$_2$ could participate, especially under blue light irradiation (450–500 nm). Several studies have reported that ^{1}O$_2$ could be photo-induced on neat and N-doped TiO$_2$ surfaces under UV and visible light absorption [77–80]. The formation of superoxide radical (O$_2^{-\cdot}$) by electronic transfer from photo-induced CB electrons to molecular oxygen is the main step, since then O$_2^{-\cdot}$ undergoes further oxidation by VB holes yielding ^{1}O$_2$. The potential to drive this [81] oxidative reaction is around +0.34 V (vs NHE at pH 7.0) [82].

In 2004 Mrowetz et al. [83] suggested for the first time the low oxidative power of N-doped TiO$_2$ under visible light irradiation. Authors related this fact to the low oxidation potential of photo-induced holes on mid-gap states induced by N-doping. In 2009, Rengifo-Herrera et al. [84] found by spin-trapping ESR measurements that under visible light irradiation, visible-light absorbing TiO$_2$ nanoparticles modified
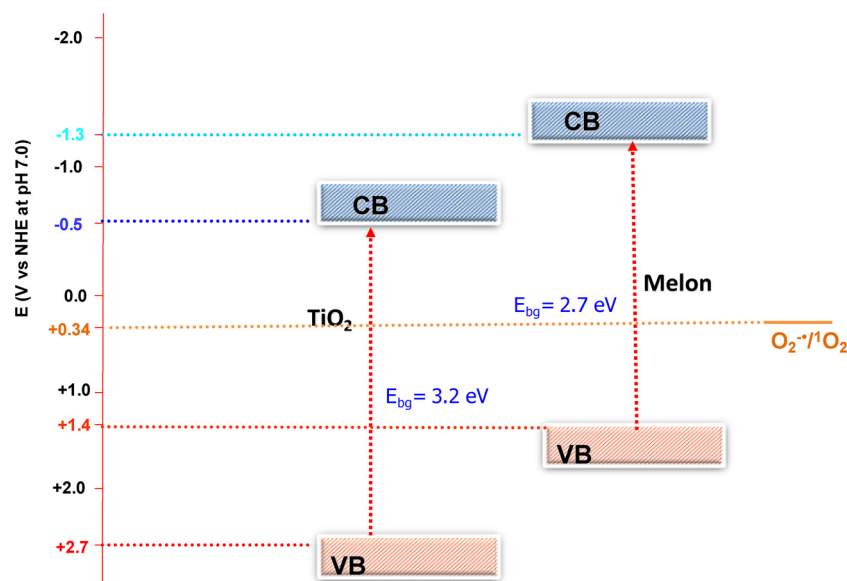
Fig. 15. Conduction band (CB) and valence band (VB) potentials of TiO_2 and melon versus normal hydrogen electrode (NHE) at pH 7.0.

with thiourea may photo-induce $^1O_2$ through the oxidation of $O_2^{-\cdot}$ by photo-induced mid-gap holes with low potential oxidation. This reaction could be thermodynamically allowed.

Now, we suggest that $^1O_2$ could be photo-induced on urea-modified TiO_2 nanoparticles, but this time, participation of mid-gap photo-induced holes would not take place. Instead of this mechanism, visible light photo-induced hole on the melon molecule (which have a low oxidation potential $+1.4$ V vs NHE) should be able to oxidize $O_2^{-\cdot}$ ($+0.34$ V vs NHE) which could be previously formed by reduction of molecular oxygen by melon CB photo-induced electrons. Recently, Wang et al. have reported by ESR-spin trapping measurements the production of singlet oxygen on g-C_3N_4 photocatalysts in aqueous solutions irradiated by sunlight. They argued that oxidation of superoxide radical by photoinduced VB holes in g-C_3N_4 could take place leading to the formation of singlet oxygen [85,86]. On the other hand, observing the redox CB potentials of melon (-1.3 V vs NHE) and TiO_2 (-0.5 V vs NHE), it seems to be possible a photo-induced electronic transfer from melon CB to TiO_2 CB. Once on TiO_2 CB, these electrons could be transferred to molecular oxygen leading to the formation of superoxide radical which could also be a source of hydroxyl radicals or singlet oxygen. Hydroxyl radicals may attack the dye molecules producing N-demethylation reactions upon visible light irradiation.

The third mechanism could involve malachite green excited states. By visible light absorption ($\lambda > 590$ nm), malachite green molecules produce excited states which could transfer photo-induced electrons to TiO_2 CB. Once these electrons are transferred on the semiconductor, they can undergo reductive reactions with molecular oxygen leading to the formation of superoxide radicals and finally $\cdot OH$ radicals, which could be responsible for the dye degradation. This mechanism has already been proposed on the literature with other dyes such as acid orange 7 and rhodamine B among others [87,88].

Regarding reusing experiments, it was observed that chitosan-UTiO$_2$ films (70QS/30UTiO$_2$-10) showed a satisfactory performance photobleaching dye stains at least after 18 h of continuous UV-A + visible light irradiation. However, by SEM micrographs and AFM images, it was evidenced that the film surface underwent some changes, especially an increase of surface roughness. This could be due to an oxidative attack of photoinduced $\cdot OH$ radicals or $^1O_2$ on the film surface leading to the partial polymer degradation.

In summary, under UV-A + visible light irradiation, the classic photocatalytic mechanism could take place, where VB photo-induced holes and hydroxyl radicals should be responsible of malachite green

degradation leading to the formation of N-demethylated byproducts. Visible light irradiation would lead to the formation of singlet oxygen through mechanisms involving dye excited states and photo-inducing e^-/h^+ pairs on melon yielding benzophenones as byproducts.

5. Conclusions

TiO_2 nanoparticles modified with urea showed visible light absorption possibly due to formation of condensed urea thermolysis byproducts such as melon. All QS/UTiO$_2$ films exhibited high malachite green photobleaching activity upon different wavelengths. When UV-A was present, classic photocatalytic processes involving VB holes or $\cdot OH$ radicals would be responsible for dye photobleaching events. Upon visible light irradiation, especially blue light (400–500 nm), a photocatalytic process, where melon light absorption would play the key role, could produce both $\cdot OH$ radicals and singlet oxygen as the main oxidative species leading to the malachite green photobleaching. Participation of dye excited states could also be responsible for photofading of dye but under light irradiation at $\lambda > 600$ nm.

Moreover, 70QS/30UTiO$_2$-10 films exhibited good dye photobleaching after 18 h of continuous UV-A + visible light irradiation. However, some surface modification of polymer was observed. This could be due to an oxidative attack of photo-induced reactive oxygen species such as OH and $^1O_2$ on the polymer structure.

Appendix A. Supplementary data

Supplementary material related to this article can be found, in the online version, at doi:https://doi.org/10.1016/j.apcatb.2018.12.004.
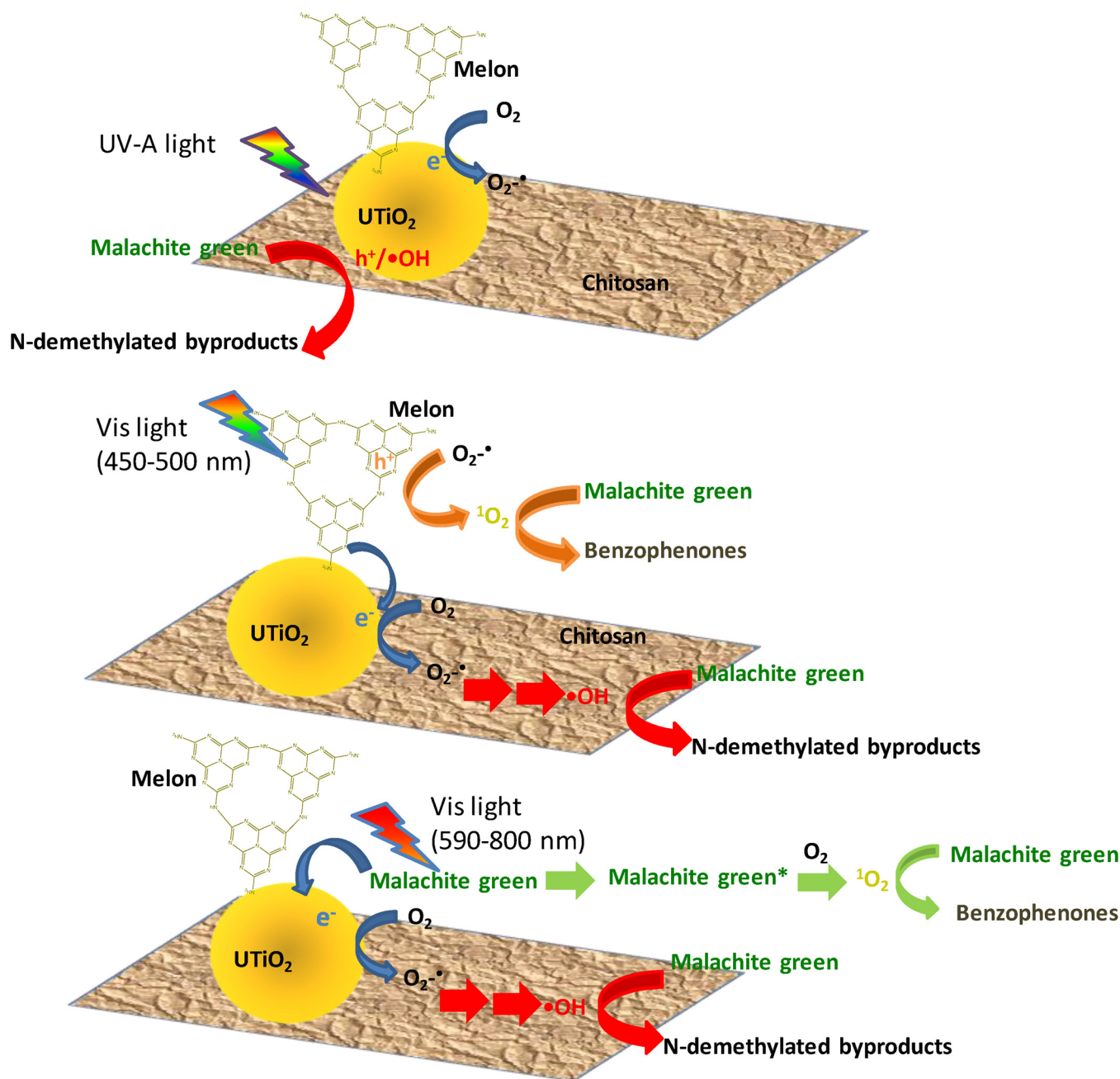
Fig. 16. Scheme showing the different photochemical and photocatalytic events responsible of dye photobleaching upon UV-A and visible light irradiation on chitosan films containing $UTiO_2$ nanoparticles.

References

[1] R. Wang, K. Hashimoto, A. Fujishima, M. Chikuni, E. Kojima, A. Kitamura, M. Shimohigoshi, T. Watanabe, Nature 388 (1997) 431–432.

[2] A.G. Agrios, P. Pichat, J. Appl. Electrochem. 35 (2005) 655–663.

[3] S. Banerjee, D.D. Dionysiou, S.C. Pillai, Appl. Catal. B Environ. 176–177 (2015) 396–428.

[4] M. Pelaez, N.T. Nolan, S.C. Pillai, M.K. Seery, P. Falaras, A.G. Kontos, P.S.M. Dunlop, J.W.J. Hamilton, J.A. Byrne, K. O'Shea, M.H. Entezari, D.D. Dionysiou, Appl. Catal. B Environ. 125 (2012) 331–349.

[5] V. Etacheri, C. Di Valentin, J. Schneider, D. Bahnemann, S.C. Pillai, J. Photochem. Photobiol. C Photochem. Rev. 25 (2015) 1–29.

[6] R. Liu, X. Zhou, F. Yang, Y. Yu, Appl. Surf. Sci. 319 (2014) 50–59.

[7] D. Li, S. Zeng, M. He, A.Z. Gu, Environ. Sci. Technol. 50 (2016) 3193–3201.

[8] Y.F. Li, D. Xu, J. Il Oh, W. Shen, X. Li, Y. Yu, ACS Catal. 2 (2012) 391–398.

[9] L.G. Devi, R. Kavitha, Appl. Catal. B Environ. 140–141 (2013) 559–587.

[10] M.V. Dozzi, E. Selli, J. Photochem. Photobiol. C Photochem. Rev. 14 (2013) 13–28.

[11] C. Di Valentin, G. Pacchioni, Catal. Today 206 (2013) 12–18.

[12] R. Asahi, T. Morikawa, H. Irie, T. Ohwaki, Chem. Rev. 114 (2014) 9824–9852.

[13] S.A. Bakar, C. Ribeiro, J. Photochem. Photobiol. C Photochem. Rev. 27 (2016) 1–29.

[14] J. Freitag, A. Domínguez, T.A. Niehaus, A. Hülsewig, R. Dillert, T. Frauenheim, D.W. Bahnemann, J. Phys. Chem. C 119 (2015) 4488–4501.

[15] J. Zhang, Y. Wu, M. Xing, S. Ahmed, K. Leghari, S. Sajjad, Energy Environ. Sci. 3 (2010) 715–726.

[16] S. Sato, Chem. Phys. Lett. 123 (1986) 126–128.

[17] F.E. Oropeza, J. Harmer, R.G. Egdell, R.G. Palgrave, Phys. Chem. Chem. Phys. (2010) 960–969.

[18] A. Kachina, E. Puzenat, S. Ould-Chikh, C. Geantet, P. Delichere, P. Afanasiev, Chem. Mater. 24 (2012) 636–642.

[19] T. Jia, F. Fu, D. Yu, J. Cao, G. Sun, Appl. Surf. Sci. 430 (2018) 438–447.

[20] L. Zeng, Z. Lu, J. Yang, M. Li, W. Song, C. Xie, Appl. Catal. B Environ. 166–167 (2015) 1–8.

[21] R. Asahi, T. Morikawa, T. Ohwaki, K. Aoki, Y. Taga, Science (80-.) 293 (2001) 269–271.

[22] S. Livraghi, A.M. Czoska, M.C.Ã. Paganini, E. Giamello, J. Solid State Chem. 182 (2009) 160–164.

[23] C. Di Valentin, G. Pacchioni, A. Selloni, S. Livraghi, V.R. Cozzi, J. Phys. Chem. B 109 (2005) 11414–11419.

[24] C. Di Valentin, E. Finazzi, G. Pacchioni, A. Selloni, S. Livraghi, M.C. Paganini, E. Giamello, Chem. Phys. 339 (2007) 44–56.
[25] S. Livraghi, M.R. Chierotti, E. Giamello, G. Magnacca, M.C. Paganini, G. Cappelletti, C.L. Bianchi, October (2008).
[26] S. Livraghi, M. Pelaez, J. Biedrzycki, I. Corazzari, E. Giamello, D.D. Dionysiou, Catal. Today 209 (2013) 54–59.
[27] D. Mitoraj, H. Kisch, Angew. Chem. - Int. Ed. 47 (2008) 9975–9978.
[28] D. Mitoraj, R. Beránek, H. Kisch, Photochem. Photobiol. Sci. 9 (2010) 31–38.
[29] X. Wang, K. Maeda, A. Thomas, K. Takanabe, G. Xin, J.M. Carlsson, K. Domen, M. Antonietti, Nat. Mater. 8 (2009) 76–80.
[30] Z. Zhao, Y. Sun, F. Dong, Nanoscale 7 (2015) 15–37.
[31] W.J. Ong, L.L. Tan, Y.H. Ng, S.T. Yong, S.P. Chai, Chem. Rev. 116 (2016) 7159–7329.
[32] H. Irie, S. Washizuka, N. Yoshino, K. Hashimoto, Chem. Commun. (Camb.) (2003) 1298–1299.
[33] J. Premkumar, Chem. Mater. 16 (2004) 3980–3981.
[34] S. Kimiagar, M.R. Mohammadizadeh, Eur. Phys. J.-Appl. Phys. 61 (2013) 1–5.
[35] V. Vaiano, G. Sarno, P. Ciambelli, D. Sannino, J. Adv. Oxid. Technol. 17 (2014) 193–201.
[36] D. Kusano, M. Emori, H. Sakama, RSC Adv. 7 (2017) 1887–1898.
[37] Y. Zhiyong, D. Laub, M. Bensimon, J. Kiwi, Inorg. Chim. Acta 361 (2008) 589–594.
[38] R. Fateh, R. Dillert, D.W. Bahnemann, (2014).
[39] L. Wu, Y. Yu, J. Zhi, RSC Adv. 5 (2015).
[40] J. Li, J. Zheng, J. Zhang, J. Feng, J. Nanosci. Nanotechnol. 16 (2016) 5875–5879.
[41] E. Rabea, M. Badawi, C. Stevens, G. Smagghe, W. Steurbaut, Biomarcromolecules 4 (2003) 1457–1465.
[42] M.A. Nawi, A.H. Jawad, S. Sabar, W.S.W. Ngah, Desalination 280 (2011) 288–296.
[43] D. Archana, B.K. Singh, J. Dutta, P.K. Dutta, Carbohydr. Polym. 95 (2013) 530–539.
[44] Y. Haldorai, J. Shim, Polym. Compos. 35 (2014) 101–113.
[45] T. Kamal, Y. Anwar, S.B. Khan, M.T.S. Chani, A.M. Asiri, Carbohydr. Polym. 148 (2016) 153–160.
[46] S. Afzal, E.M. Samsudin, L.K. Mun, N.M. Julkapli, S.B.A. Hamid, Mater. Res. Bull. 86 (2017) 24–29.
[47] J.A. Rengifo-Herrera, D.A. Marín-Silva, E. Mendoza-Portillo, A.N. Pinotti, L.R. Pizzio, Mol. Catal. 448 (2018).
[48] J. Lamarra, S. Rivero, A. Pinotti, Mater. Sci. Eng. C 67 (2016) 717–726.
[49] A. Julson, D.F. Ollis, Appl. Catal. B Environ. 65 (2006) 315–325.
[50] D. Ollis, Appl. Catal. B Environ. 242 (2019) 431–440.
[51] J.T.Y. Jr, Surf. Sci. 603 (2009) 1605–1612.
[52] S. Yin, H. Yamaki, M. Komatsu, Q. Zhang, J. Wang, Q. Tang, T. Sato, Solid State Sci. 7 (2005) 1479–1485.
[53] J. Yuan, M. Chen, J. Shi, W. Shangguan, Int. J. Hydrogen Energy 31 (2006) 1326–1331.
[54] J.A. Rengifo-Herrera, J. Kiwi, C. Pulgarin, J. Photochem. Photobiol. A: Chem. 205 (2009) 109–115.
[55] V.M. Fuchs, E.L. Soto, M.N. Blanco, L.R. Pizzio, J. Colloid Interface Sci. 327 (2008) 403–411.
[56] J.A. Rengifo-Herrera, M.N. Blanco, L.R. Pizzio, Mater. Res. Bull. 49 (2014).
[57] J.A. Rengifo-Herrera, L.R. Pizzio, M.N. Blanco, C. Roussel, C. Pulgarin, Photochem. Photobiol. Sci. 10 (2011) 29–34.
[58] L. Yong, G. Zhanqi, J. Yuefei, H. Xiaobin, S. Cheng, Y. Shaogui, W. Lianhong,

W. Qingeng, F. Die, J. Hazard. Mater. 285 (2015) 127–136.
[59] B.P. Cho, T. Yang, L.R. Blankenship, J.D. Moody, M. Churchwell, F. a Beland, S.J. Culp, Chem. Res. Toxicol. 16 (2003) 285–294.
[60] D.F. Duxbury, Chem. Rev. 93 (1993) 381–433.
[61] N. Kuramoto, T. Kitao, Dyes Pigm. 3 (1982) 49–58.
[62] Y. Nosaka, M. Matsushita, J. Nishino, A.Y. Nosaka, Sci. Technol. Adv. Mater. 6 (2005) 143–148.
[63] A.M. Bernhard, D. Peitz, M. Elsener, A. Wokaun, O. Kröcher, Appl. Catal. B Environ. 115–116 (2012) 129–137.
[64] A.M. Bernhard, D. Peitz, M. Elsener, T. Schildhauer, O. Kröcher, Catal. Sci. Technol. 3 (2013) 942–951.
[65] A.M. Bernhard, I. Czekaj, M. Elsener, O. Kröcher, Appl. Catal. B Environ. 134–135 (2013) 316–323.
[66] X.-X. Zou, G.-D. Li, Y.-N. Wang, J. Zhao, C. Yan, M.-Y. Guo, L. Li, J.-S. Chen, Chem. Commun. (Camb.) 47 (2011) 1066–1068.
[67] K. Sridharan, E. Jang, T.J. Park, Appl. Catal. B Environ. 142–143 (2013) 718–728.
[68] A. Thomas, A. Fischer, F. Goettmann, M. Antonietti, J.-O. Müller, R. Schlögl, J.M. Carlsson, J. Mater. Chem. 18 (2008) 4893.
[69] T.S. Miller, A.B. Jorge, T.M. Suter, A. Sella, F. Corà, P.F. McMillan, Phys. Chem. Chem. Phys. 19 (2017) 15613–15638.
[70] S.J. Yang, J.H. Cho, G.H. Oh, K.S. Nahm, C.R. Park, Carbon 47 (2009) 1585–1591.
[71] T.P. Ang, Y.M. Chan, J. Phys. Chem. C 115 (2011) 15965–15972.
[72] B.V. Lotsch, M. Döblinger, J. Sehnert, L. Seyfarth, J. Senker, O. Oeckler, W. Schnick, Chem. - A Eur. J. 13 (2007) 4969–4980.
[73] V.W.H. Lau, I. Moudrakovski, T. Botari, S. Weinberger, M.B. Mesch, V. Duppel, J. Senker, V. Blum, B.V. Lotsch, Nat. Commun. 7 (2016) 1–15.
[74] A.P. Dementjev, A. De Graaf, M.C.M. Van de Sanden, K.I. Maslakov, A.V. Naumkin, A.A. Serov, Diam. Relat. Mater. 9 (2000) 1904–1907.
[75] J.A. Rengifo-Herrera, E. Mielczarski, J. Mielczarski, N.C. Castillo, J. Kiwi, C. Pulgarin, Appl. Catal. B Environ. 84 (2008) 448–456.
[76] P. Cheng, P. Deng, M. Gu, X. Dai, Mater. Chem. Phys. 107 (2008) 77–81.
[77] K. Hirakawa, T. Hirano, Chem. Lett. 35 (2006) 832–833.
[78] T. Daimon, Y. Nosaka, Luminescence (2007) 4420–4424.
[79] T. Daimon, T. Hirakawa, M. Kitazawa, J. Suetake, Y. Nosaka, Appl. Catal. A Gen. 340 (2008) 169–175.
[80] K. Naito, T. Tachikawa, T. Fujitsuka, T. Majima, J. Phys. Chem. C 112 (2008) 1048–1059.
[81] T. Hirakawa, T. Daimon, M. Kitazawa, N. Ohguri 190 (2007) 58–68.
[82] T. Sawyer, S. Valentine, Acc. Chem. Res. (1981) 393–400.
[83] M. Mrowetz, W. Balcerski, A.J. Colussi, M.R. Hoffmann, J. Phys. Chem. B 108 (2004) 17269–17273.
[84] J.A. Rengifo-Herrera, K. Pierzchała, A. Sienkiewicz, L. Forró, J. Kiwi, C. Pulgarin, Appl. Catal. B Environ. 88 (2009) 398–406.
[85] F. Wang, Y. Feng, P. Chen, Y. Wang, Y. Su, Q. Zhang, Y. Zeng, Z. Xie, H. Liu, Y. Liu, W. Lv, G. Liu, Appl. Catal. B Environ. 227 (2018) 114–122.
[86] F. Wang, Y. Wang, Y. Feng, Y. Zeng, Z. Xie, Q. Zhang, Y. Su, P. Chen, Y. Liu, K. Yao, W. Lv, G. Liu, Appl. Catal. B Environ. 221 (2018) 510–520.
[87] M. Stylidi, D.I. Kondarides, X.E. Verykios, Appl. Catal. B Environ. 40 (2003) 271–286.
[88] J. Zhao, C. Chen, W. Ma, Top. Catal. 35 (2005) 269–278.